catalysts

MDPI

Article

Controllable Construction of IrCo Nanoclusters and the Performance for Water Electrolysis

Fangqin Mao, Xiaojie Zhao, Ying Chang * and Jingchun Jia *

College of Chemistry and Environmental Science, Inner Mongolia Key Laboratory of Green Catalysis and Inner Mongolia Collaborative Innovation Center for Water Environment Safety, Inner Mongolia Normal University, Hohhot 010022, China

* Correspondence: changying@imnu.edu.cn (Y.C.); jjc1983@126.com (J.J.)

Abstract: Finding a suitable catalyst is an important research direction in hydrogen (H_2) production from water electrolysis. We report a synthetic method to obtain Ir_xCo/C clusters by polyol reduction. The catalyst is small in size and can be evenly distributed. The Ir_3Co/C cluster catalyst had very good activity under acidic conditions. The overpotential of the best-performing Ir_3Co/C cluster for the oxygen evolution reaction (OER) and the hydrogen evolution reaction (HER) is only 290 mV and 91 mV when 10 mA cm^{-2} and 100 mA cm^{-2}. The catalyst performance may be improved because of the synergistic effect and the small size of the prepared catalyst, which accelerates proton transfer. This approach offers a strategy to reduce costs while improving catalytic activity.

Keywords: electrolysis; nanoclusters; Ir-based catalysts

check for updates

Citation: Mao, F.; Zhao, X.; Chang, Y.; Jia, J. Controllable Construction of IrCo Nanoclusters and the Performance for Water Electrolysis. *Catalysts* **2022**, *12*, 914. https://doi.org/10.3390/catal12080914

Academic Editor: Svetlana B. Štrbac

Received: 31 July 2022
Accepted: 15 August 2022
Published: 19 August 2022
Corrected: 14 November 2022

1. Introduction

Hydrogen is an ideal source of energy; an important step in harnessing it is to develop ultra-stable and efficient technology [1]. Among the many preparation methods, the electrolysis of water is a promising approach [2,3]. It includes the anodic oxygen evolution reaction and the cathodic hydrogen evolution reaction. However, the weak point is that the anodic oxygen evolution reaction has a large overpotential and slow kinetics [4,5].

Among catalysts, noble metals have very good catalytic activity. Ir-based catalysts are considered to be excellent materials for the OER under alkaline conditions [6,7]. Nevertheless, due to their high price, slow kinetics under acidic conditions, and easy corrosion [8], Ir-based catalysts are not widely used. Until now, researchers have used a number of different methods to improve catalytic performance. For example, the prepared structures include three-dimensional porous [9] catalysts; core–shell [10] structures; and cubic nanocage [11] structures; deposited Ni-P films [12], embedded on copper foam [13]; and doping transition metals [14] in noble metal catalysts. These methods proved that the reasonable design of catalysts can significantly improve their catalytic effects.

Therefore, researchers have performed many related studies. For the material, it is mainly the introduction of a second component to enhance OER catalysis [15–17]. Bimetallic alloys, such as Ir-Ni [18], Ir-Ru [19], and FeCo [20], have been shown to have significantly improved water electrolysis performance. The improved performance is due to the synergistic effect between metals, which can reduce the adsorption energy of intermediates. In the synthesis procedure, clusters prepared by traditional methods are easy to condense. However, recent research has shown that loading the catalyst on the carbon layer [21,22] can overcome this deficiency.

It is on the basis of these studies that we chose to study transition metal-doped precious metal (cobalt (Co))-doped Ir). For the synthesis method, we used the oil bath method to synthesize Ir_xCo cluster catalysts by adjusting the proportion of metal precursors. Considering the influence of catalyst size on the performance of the catalyst, we prepared the catalyst on the nanometer scale. The reduction in the catalyst size allows the electrolyte

to contact the catalyst more fully and catalyze the reaction. The prepared clusters are uniformly distributed on the thin carbon layer (Ir_xCo/C). This is expected to promote the industrial development of water electrolysis for hydrogen production.

2. Results and Discussion

By reducing the polyols and adjusting the ratio of the Ir and Co precursors, different proportions of the Ir_xCo/C (x = 1, 2, 3) clusters can be obtained (see Figure S1 and Experimental section). First, the crystallinity of the Ir_3Co/C cluster and XC-72R was measured and compared by X-ray diffraction (XRD) (Figure 1a). On the one hand, it was found that there were no characteristic peaks of other metals in the sample, but only the characteristic peaks of carbon at 24.5° and 44.5°. This may be due to the fact that the scanning rate was too fast during the XRD analysis, resulting in the absence of the corresponding characteristic peaks. Alternatively, the Ir_3Co/C cluster itself may have an amorphous structure. On the other hand, when the sample contains more Co, the change in half peak width is opposite to the decrease of peak strength (Figure S2), indicating that the nanoparticles have lower crystallinity and a smaller crystal size [23]. From another point of view, the peak strength of clusters decreases greatly, which indicates that clusters are successfully loaded on the carbon support, which further proves the synergistic effect of replacing Ir with Co on catalyst performance.

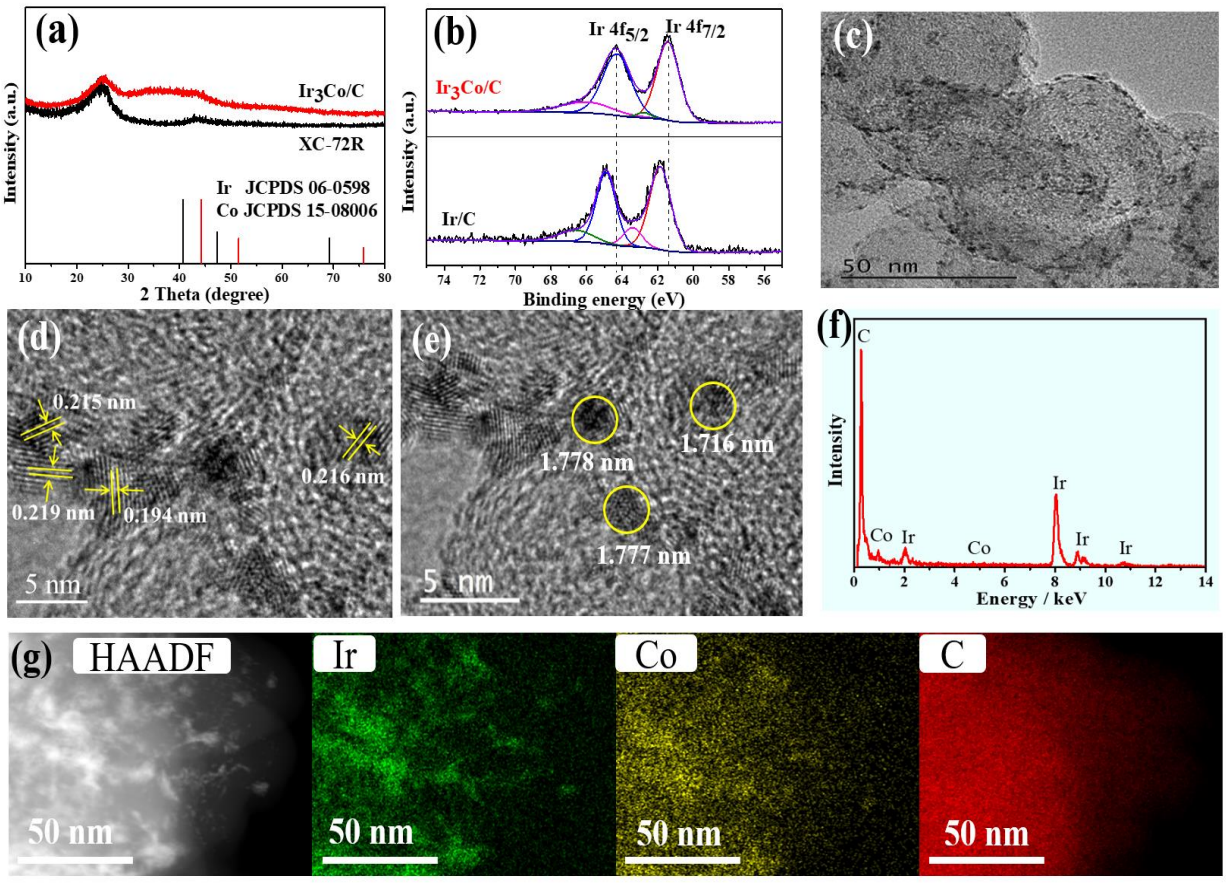

Figure 1. (**a**) XRD characterizations of Ir_3Co/C and XC-72R. (**b**) XPS images of Ir_3Co/C and Ir/C. (**c**) TEM image and (**d**,**e**) HRTEM diagram of Ir_3Co/C. (**f**) EDS spectrum. (**g**) HAADF-STEM image of Ir_3Co/C, from left to right are STEM-EDS mappings of Ir, Co, and C.

X-ray photoelectron spectroscopy (XPS) was used to record the structure of Ir_3Co/C clusters (Figure S3). From Figure 1b, we can see that Ir in Ir_3Co/C has a partial negative charge because, compared to Ir/C, its characteristic peak is shifted to the right, the lower binding energy end. In addition, as shown in Figure S4, compared with Ir_3Co/C, the Ir

4f peak of Ir/C shifts to the end with higher binding energy. From Figure S3a, it can be seen that the sample has O 1s, C 1s, and Ir 4f peaks, which proves that the sample contains oxygen, carbon, and iridium elements. As for the peak of O 1s, it may be due to partial oxidation of samples exposed to air. It can be seen from the Ir 4f spectrum of the Ir_3Co/C sample that Ir has two valence states, namely Ir^0 and Ir^{4+} (Figure S3b). As shown in Figure S3c, the peak of Co 2p is very disordered, due to the small amount of Co in the sample, which leads to a low probability of Co detection. In Figure S3d, it is shown that the carbon bond types in the sample are alternating single and double bonds.

The Ir_3Co/C clusters were detected by transmission electron microscopy (TEM). It can be seen from Figure 1c that the sample is evenly distributed on the carbon carrier. From Figure 1d, the yellow markings show that the particle has continuous lattice fringe, of which the corresponding crystal planes are (111) and (200). From Figure 1e, the size of the crystal is 1.7–1.8 nm, indicating that the prepared crystal is similarly very uniform. Figure 1f shows the electron diffraction spectrum (EDS) of Ir_3Co/C. The appearance of characteristic peaks indicate the presence of C, Ir, and Co, with the highest content of C. The presence of these elements was also demonstrated by high-angle annular dark field scanning TEM (HAADF-STEM) (Figure 1g). This is consistent with the conclusion obtained from the electron diffraction spectrum.

Ir-based catalysts are widely used in energy and environmental applications due to face-centered-cubic (fcc) structure [24,25]. However, its performance is hampered in acidic conditions. Thus, it is necessary to seek a catalyst with excellent performance under acidic conditions. The OER polarization curves of catalysts under acidic conditions are shown in Figure 2a. The required overpotentials are 446, 338, 360, 328, and 290 mV for Pt/C, IrCo/C, Ir_2Co/C, Ir/C, and Ir_3Co/C when the current density is 10 mA cm^{-2} (Figure 2b). The minimum value of 290 mV indicated that Ir_3Co/C had the best catalytic performance, which was less than Ir/C (38 mV). Table S3 shows the performance comparison of these catalysts. The comparison of the OER performance of Ir_3Co/C with IrO_2 and RuO_2 under acidic conditions is shown in Table S4. When the Co content is optimal, the polarization curve shows a lower overpotential, which is mainly due to the synergistic interaction between Ir and Co. The Tafel slope also confirms this viewpoint. The Tafel slopes of Pt/C, IrCo/C, Ir_2Co/C, Ir/C, and Ir_3Co/C are 187.84, 65.40, 65.21, 51.67, and 50.27 mV dec^{-1} (Figure 2c). Ir_3Co/C has the lowest Tafel slope, indicating that the catalytic OER reaction kinetics were very fast. In addition, compared with its electron transfer impedance (R_{ct}), the Ir_3Co/C has the smallest electron transfer impedance (Figure 2d). The activity can be evaluated by the electrochemically active surface area (ECSA) (Figure S5). The C_{dl} of Ir_3Co/C is 39.61 mF cm^{-2} (Figure S6), which is the highest among all the samples. This means that it can expose more active sites, thus speeding up the reaction. This result suggests that the intrinsic OER activities for Pt/C, Ir_2Co/C, IrCo/C, Ir/C, and Ir_3Co/C increased in order. Combined with the above results, Ir_3Co/C has good catalytic performance, and has great application prospect.

The prepared catalyst was also tested OER performance under alkaline conditions. The polarization curve of Ir_3Co/C is furthest to the left (Figure S7a), which means the least polarization occurred. The overpotential is only 310 mV (Figure S7b), the lowest C_{dl} is found (Figure S7c), and the double layer capacitance is only 7.50 mF cm^{-2} (Figure S7d), which is the largest among various catalysts. Through the test, we found that the catalytic effect of Ir_3Co/C decreased slightly under alkaline conditions, but was still higher than the samples of Ir/C and Pt/C. These results indicate that Ir_3Co/C has a better catalytic effect under acidic conditions.

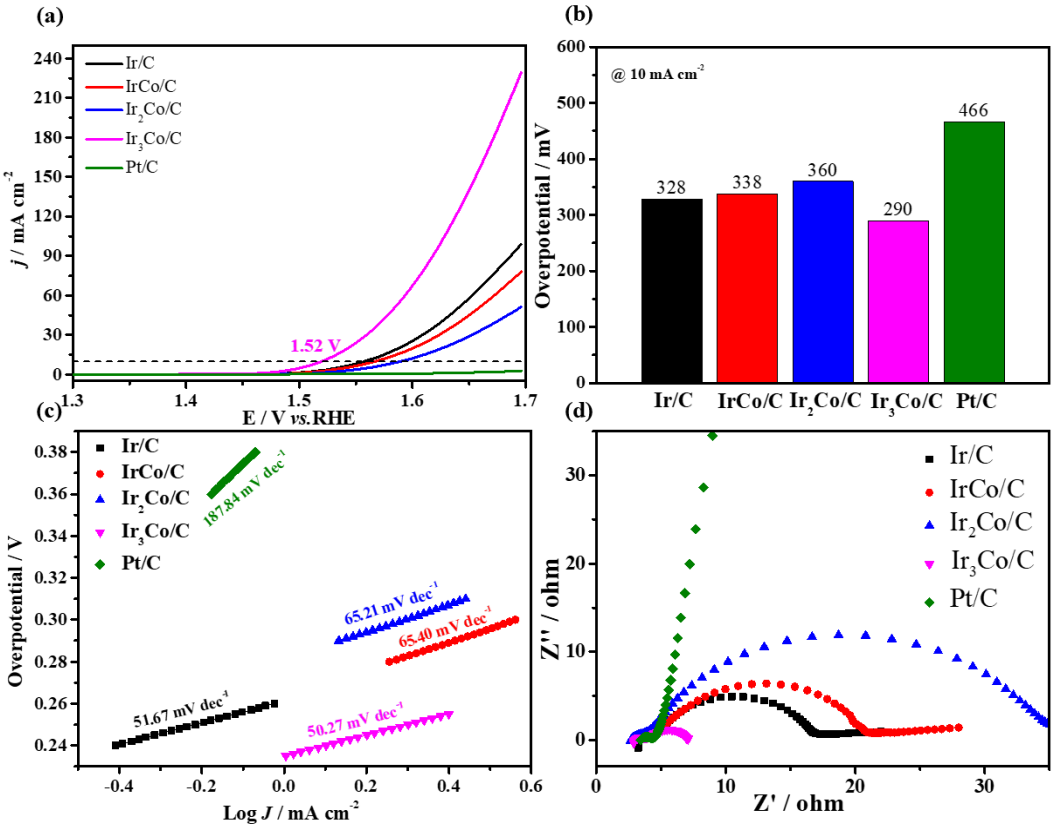

Figure 2. Electrochemical test results of different catalysts. (**a**) Polarization curves of OER in 0.5 M H_2SO_4. (**b**) The overpotential required to reach 10 mA cm^{-2}. (**c**) The corresponding Tafel slopes. (**d**) EIS.

The hydrogen evolution reaction of the prepared catalyst was further tested under acidic conditions. Pt-based catalysts are considered to be the best catalysts for HER [26], on account of their low overpotential and excellent reaction kinetics. The polarization curves of HER under acidic medium is shown in Figure 3a. It can be found that the polarization curve of Ir_3Co/C is very close to Pt/C. Figure 3b shows that the overpotential of Ir_3Co/C is much lower than those of the catalysts, except Pt/C, indicating its outstanding activities with only a 91 mV overpotential at 100 mA cm^{-2}. The lower charge-transfer resistance (Figure 3c) also proves its excellence. The C_{dl} of Ir_3Co/C is between Pt/C and Ir/C (Figure 3d). Then, we tested the HER of the catalyst under alkaline conditions. The polarization curve in Figure S8a shows that the catalyst achieves high current density. This is because the background current is so high that it has a very high initial potential. When the current density reaches 100 mA cm^{-2}, the overpotential of Ir_3Co/C is only 84 mV (Figure S8b), which is very small. In addition, its C_{dl} is higher than other catalysts (Figure S8d), although the downside is that its electrochemical impedance is very large (Figure S8c), indicating that its reaction speed is slow. In summary, Ir_3Co/C is expected to be a candidate for a high-efficiency catalyst for water electrolysis, especially under acidic conditions, with excellent performance.

Compared with some previous catalysts (Tables S5 and S6), the prepared Ir_3Co/C catalysts has good catalytic performance. The main reasons for the performance improvement of the catalyst are as follows: First, a smaller nanocluster structure is formed and more active sites are generated. Second, the carbon-based carrier can effectively increase the conductivity and fix the nanoclusters. Finally, Co and Ir metals have synergistic effect that promote the occurrence of the reaction.

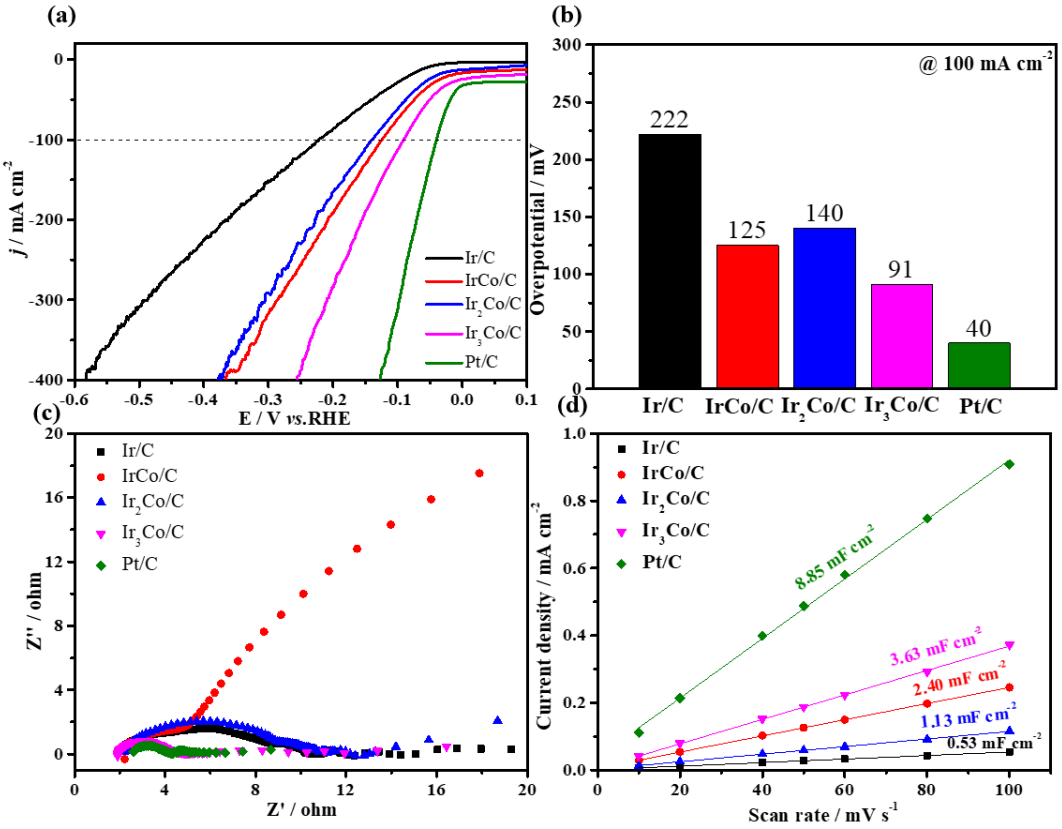

Figure 3. Electrochemical test results of different catalysts. (**a**) Polarization curves of HER in 0.5 M H_2SO_4. (**b**) The overpotential required to reach 100 mA cm^{-2}. (**c**) EIS. (**d**) Electrical double-layer capacitor (C_{dl}).

3. Materials and Methods

3.1. Experimental Materials and Material Characterization

3.1.1. Experimental Materials

All the materials were purchased from the reagent company, except the ultrapure water. The water was obtained by an ultrapure purification system. And none of them were processed. The specific materials are as follows:

Iridium$_{(III)}$ chloride hydrate ($IrCl_3$ xH_2O, A.R, Titan Corp, Shanghai, China), Cobalt$_{(II)}$ chloride hexahydrate ($CoCl_2 \cdot 6H_2O$, A.R, Titan Corp, Shanghai, China), Sodium citrate ($C_6H_5Na_3O_7$, A.R, Sinopharm group, Shanghai, China), potassium hydroxide (KOH, A.R, Sinopharm group, Shanghai, China), ethylene glycol (C_2H_5OH, A.R, Sinopharm group, Shanghai, China), sulphuric acid (H_2SO_4, Tianjin No. 3 Chemical Reagent factory, Tianjin, China),XC-72 carbon powder (Cabot Corp, Boston, USA), and Nafion (~5 wt%, Sigma-Aldrich Corp, Shanghai, China).

3.1.2. Materials Characterization

Characterizations of Crystal Structure: X-ray diffraction (XRD, Rigaku Ultima IV, Rigaku, Tokyo, Japan) (scan speed: 4° min^{-1}, 2θ range: 5–90°) to observe the crystal structure of the catalysts.

Characterizations of Surface Composition: X-ray photoelectron spectroscopy (XPS, ESCALAB 250Xi, Thermo Fisher Scientific, Waltham, MA, USA) to study the surface composition of the catalysts.

Characterizations of Morphology and Structure: The morphology and structure of the catalysts were characterized by Transmission electron microscopy (TEM, FEI Tecnai G2 F20, Thermo Fisher Scientific, Waltham, MA, USA) and High-resolution TEM (HRTEM, FEI Tecnai G2 F30, Thermo Fisher Scientific, Waltham, MA, USA).

3.1.3. Preparation of Working Electrode

- Nafion (5%), ultra-pure water and ethanol were used to prepare slurry at 1:9:10.
- 5 mg catalyst was mixed with 1 mL of the slurry.
- Ultrasonic to uniform dispersion.
- The pipette gun was used to take 16 μL of the slurry and uniformly add it to the carbon paper with an area of 0.25 cm^2.
- The working electrode load obtained was 0.32 mg cm^{-2}.

3.2. Material Synthesis

For the Ir_3Co/C, 40 mg $C_6H_5Na_3O_7$ and 30 mL ethylene glycol were placed into identical round-bottomed flasks and ultrasonicated to fully dissolve sodium citrate. Then, 2168 μL $IrCl_3 \cdot xH_2O$ (0.1 g mL^{-1}) solution and 268 μL $CoCl_2 \cdot 6H_2O$ (0.2 g mL^{-1}) solution was measured by a pipette and placed into a distillation flask. The flask was placed on a magnetic stirrer and a stirrer bar was added to ensure that the solution was stirred evenly. Then, the pH of solution was adjusted to 9 by using 1 M KOH, and 40 mg XC-72 carbon powder was added to conduct ultrasound. After the ultrasonication (Ningbo Xinzhi Biotechnology Co., LTD., Ningbo, China), the solution was placed into an oil bath with a magnetic stirrer (Germany IKA Co., LTD., ZheJiang, China). The speed and temperature were set to 300 rpm and 160 °C, and the reaction lasted for four hours. After the acquired catalyst was cooled completely, it was filtered, washed with ultrapure water, and dried in a blast oven (Shanghai Yiheng Science & Technology Co., LTD., Shanghai, China) for 8 h. Finally, after the sample was sufficiently dried, it was ground to obtain the required catalyst. The preparation methods for the rest of the samples were the same, except for the different amounts used.

3.3. Electrochemical Measurements

The electrochemical test were performed via the three-electrode system in the CHI 760E electrochemical workstation (Chenhua, Shanghai, China). The working electrode was carbon paper (area: 0.25 cm^2) supported by the catalyst; the counter electrode was a carbon rod; and the reference electrode was Ag/AgCl (acidic conditions) or Hg/HgO (alkaline conditions). Linear sweep curve (LSV) (sweep rate: 5 mV s^{-1}), cyclic voltammetry curve (CV) (sweep rate: 10, 20, 40, 50, 60, 80, and 100 mV s^{-1}), and electrochemical alternating impedance (EIS) (potential: 1.4 V, frequency range: 100-0.01 Hz) were utilized to test electrochemical performance. The acidic and alkaline solutions were 0.5 M H_2SO_4 and 1 M KOH. The data obtained were corrected against the reversible hydrogen electrode (RHE).

4. Conclusions

In brief, Ir_xCo/C clusters were synthesized by a simple method. The size of Ir_3Co/C clusters was 1.7–1.8 nm. The abundance of active sites increased its catalytic activity. Ir_3Co/C has excellent performance under different pH conditions. The OER was best under acidic conditions, with an overpotential of 290 mV at 10 mA cm^{-2}. It also had very good HER performance, with an overpotential of 91 mV at 100 mA cm^{-2}. Therefore, the catalyst is expected to be used as a bifunctional catalyst. This provides a method to increase the activity of a catalyst while reducing the cost. Therefore, it has broad application prospects in the process of water electrolysis.

Supplementary Materials: The following supporting information can be downloaded at: https://www.mdpi.com/article/10.3390/catal12080914/s1, Figure S1: Synthesis diagram of Ir_xCo clusters was prepared by oil bath; Figure S2: XRD patterns of XC-72R Vulcan carbon, Ir/C, IrCo/C, Ir_2Co/C and Ir_3Co/C; Figure S3: XPS spectra of Ir_3Co/C: (a) survey, (b) Ir 4f, (c) Co 2p, (d) C 1s; Figure S4: XPS spectra of Ir/C: (a) survey, (b) Ir 4f, (c) C 1s; Figure S5: CV curves at different scan rates (10, 20, 40, 50, 60, 80 and 100 mV s^{-1}) for (a) IrCo/C, (b) Ir_2Co/C, (c) Ir_3Co/C, (d) Ir/C; Figure S6: Electrical double layer capacitor (C_{dl}) of the OER in 0.5 M H_2SO_4; Figure S7: (a) LSV curves of the OER in 1 M KOH. (b) The overpotential at 10 mA cm^{-2}. (c) EIS results of the catalysts.

(d) Electrical double layer capacitor (C_{dl}); Figure S8: (a) LSV curves of the HER in 1 M KOH. (b) The overpotential at 100 mA cm^{-2}. (c) EIS results of the catalysts. (d) Electrical double layer capacitor (C_{dl}); Table S1. Main reagents in the experiment; Table S2. Main instruments of the experiment; Table S3: Comparison of different catalysts; Table S4: Comparison of the OER performance of IrO_2 and RuO_2 with Ir_3Co/C [8,27]; Table S5: OER electrocatalysts reported recently [19,28–31]; Table S6. HER electrocatalysts reported recently [32–36].

Author Contributions: Formal analysis, F.M. and X.Z; investigation, F.M. and X.Z; data curation, F.M. and X.Z.; writing—original draft preparation, F.M.; writing—review and editing, Y.C. and J.J.; supervision, Y.C. and J.J; funding acquisition, J.J. All authors have read and agreed to the published version of the manuscript.

Funding: We would like to thank Science and Technology Program of Inner Mongolia Autonomous Region, China (2020PT0003), and the Research Foundation for Advanced Talents of Inner Mongolia Normal University (No.2018YJRC001, 2018YJRC012) for financial support.

Data Availability Statement: Not applicable.

Conflicts of Interest: The authors declare no conflict of interest.

References

1. Cui, X.; Chen, M.; Xiong, R.; Sun, J.; Liu, X.; Geng, B. Ultrastable and efficient H_2 production via membrane-free hybrid water electrolysis over a bifunctional catalyst of hierarchical Mo–Ni alloy nanoparticles. *J. Mater. Chem. A* **2019**, *7*, 16501–16507. [CrossRef]
2. Chen, L.-W.; Liang, H.-W. Ir-based bifunctional electrocatalysts for overall water splitting. *Catal. Sci. Technol.* **2021**, *11*, 4673–4689. [CrossRef]
3. Qazi, U.Y.; Javaid, R.; Tahir, N.; Jamil, A.; Afzal, A. Design of advanced self-supported electrode by surface modification of copper foam with transition metals for efficient hydrogen evolution reaction. *Int. J. Hydrog. Energy* **2020**, *45*, 33396–33406. [CrossRef]
4. Yang, F.; Chen, X.; Li, Z.; Wang, D.; Liu, L.; Ye, J. Ultrathin FeP nanosheets as an efficient catalyst for electrocatalytic water oxidation: Promoted intermediates adsorption by surface defects. *ACS Appl. Energy Mater.* **2020**, *3*, 3577–3585. [CrossRef]
5. Tian, L.; Zhai, X.; Wang, X.; Li, J.; Li, Z. Advances in manganese-based oxides for oxygen evolution reaction. *J. Mater. Chem. A* **2020**, *8*, 14400–14414. [CrossRef]
6. Alia, S.M.; Shulda, S.; Ngo, C.; Pylypenko, S.; Pivovar, B.S. Iridium-based nanowires as highly active, oxygen evolution reaction electrocatalysts. *ACS Catal.* **2018**, *8*, 2111–2120. [CrossRef]
7. Jiang, P.; Chen, J.; Wang, C.; Yang, K.; Gong, S.; Liu, S.; Lin, Z.; Li, M.; Xia, G.; Yang, Y.; et al. Tuning the activity of carbon for electrocatalytic hydrogen evolution via an Iridium-Cobalt alloy core encapsulated in nitrogen-doped carbon cages. *Adv. Mater.* **2018**, *30*, 1705324. [CrossRef]
8. Zhao, X.; Chang, Y.; Ji, J.; Jia, J.; Jia, M. Ultradispersed IrxNi clusters as bifunctional electrocatalysts for high-efficiency water splitting in acid electrolytes. *RSC Adv.* **2021**, *11*, 33179–33185. [CrossRef]
9. Zhao, Y.; Luo, M.; Chu, S.; Peng, M.; Liu, B.; Wu, Q.; Liu, P.; de Groot, F.M.F.; Tan, Y. 3D nanoporous iridium-based alloy microwires for efficient oxygen evolution in acidic media. *Nano Energy* **2019**, *59*, 146–153. [CrossRef]
10. Wang, H.; Chen, Z.N.; Wu, D.; Cao, M.; Sun, F.; Zhang, H.; You, H.; Zhuang, W.; Cao, R. Significantly enhanced overall water splitting performance by partial oxidation of Ir through Au modification in core-shell alloy structure. *J. Am. Chem. Soc.* **2021**, *143*, 4639–4645. [CrossRef]
11. Zhu, J.; Chen, Z.; Xie, M.; Lyu, Z.; Chi, M.; Mavrikakis, M.; Jin, W.; Xia, Y. Iridium-based cubic nanocages with 1.1-nm-thick walls: A highly efficient and durable electrocatalyst for water oxidation in an acidic medium. *Angew. Chem. Int. Ed.* **2019**, *58*, 7244–7248. [CrossRef] [PubMed]
12. Battiato, S.; Bruno, L.; Terrasi, A.; Mirabella, S. Superior performances of electroless-deposited Ni–P films decorated with an ultralow content of Pt for water-splitting reactions. *ACS Appl. Energy Mater.* **2022**, *5*, 2391–2399. [CrossRef]
13. Qazi, U.Y.; Javaid, R.; Zahid, M.; Tahir, N.; Afzal, A.; Lin, X.-M. Bimetallic NiCo–$NiCoO_2$ nano-heterostructures embedded on copper foam as a self-supported bifunctional electrode for water oxidation and hydrogen production in alkaline media. *Int. J. Hydrog. Energy* **2021**, *46*, 18936–18948. [CrossRef]
14. Wang, F.; Kusada, K.; Wu, D.; Yamamoto, T.; Toriyama, T.; Matsumura, S.; Nanba, Y.; Koyama, M.; Kitagawa, H. Solid-solution alloy nanoparticles of the immiscible Iridium-Copper system with a wide composition range for enhanced electrocatalytic applications. *Angew. Chem. Int. Ed.* **2018**, *57*, 4505–4509. [CrossRef]
15. Feng, J.; Lv, F.; Zhang, W.; Li, P.; Wang, K.; Yang, C.; Wang, B.; Yang, Y.; Zhou, J.; Lin, F.; et al. Iridium-based multimetallic porous hollow nanocrystals for efficient overall-water-splitting catalysis. *Adv. Mater.* **2017**, *29*, 1703798. [CrossRef]
16. Park, J.; Sa, Y.J.; Baik, H.; Kwon, T.; Joo, S.H.; Lee, K. Iridium-based multimetallic nanoframe@nanoframe structure: An efficient and robust electrocatalyst toward oxygen evolution reaction. *ACS Nano* **2017**, *11*, 5500–5509. [CrossRef]

17. Chang, J.; Zang, S.; Li, J.; Wu, D.; Lian, Z.; Xu, F.; Jiang, K.; Gao, Z. Nitrogen-doped porous carbon encapsulated nickel iron alloy nanoparticles, one-step conversion synthesis for application as bifunctional catalyst for water electrolysis. *Electrochim. Acta* **2021**, *389*, 138785. [CrossRef]
18. Liu, S.; Hu, Z.; Wu, Y.; Zhang, J.; Zhang, Y.; Cui, B.; Liu, C.; Hu, S.; Zhao, N.; Han, X.; et al. Dislocation-strained IrNi alloy nanoparticles driven by thermal shock for the hydrogen evolution reaction. *Adv. Mater.* **2020**, *32*, 2006034. [CrossRef]
19. Xu, J.; Li, J.; Lian, Z.; Araujo, A.; Li, Y.; Wei, B.; Yu, Z.; Bondarchuk, O.; Amorim, I.; Tileli, V.; et al. Atomic-step enriched ruthenium–iridium nanocrystals anchored homogeneously on MOF-derived support for efficient and stable oxygen evolution in acidic and neutral media. *ACS Catal.* **2021**, *11*, 3402–3413. [CrossRef]
20. Hu, H.; Lei, X.; Li, S.; Fu, L.; Peng, R.; Ren, X.; Wang, J. FeCo alloy nanoparticles obtained by PVP modified oxalate template method as an efficient oxygen evolution reaction catalyst. *J. Met.* **2021**, *74*, 346–353. [CrossRef]
21. Zhang, Q.; Yang, X.; Guan, J. Applications of magnetic nanomaterials in heterogeneous catalysis. *ACS Appl. Nano Mater.* **2019**, *2*, 4681–4697. [CrossRef]
22. Huang, Y.; Zhang, S.L.; Lu, X.F.; Wu, Z.P.; Luan, D.; Lou, X.W.D. Trimetallic spinel $NiCo_{2-x}Fe_xO_4$ nanoboxes for highly efficient electrocatalytic oxygen evolution. *Angew. Chem. Int. Ed.* **2021**, *60*, 11841–11846. [CrossRef] [PubMed]
23. Wang, Q.; Ming, M.; Niu, S.; Zhang, Y.; Fan, G.; Hu, J.-S. Scalable solid-state synthesis of highly dispersed uncapped metal (Rh, Ru, Ir) nanoparticles for efficient hydrogen evolution. *Adv. Energy Mater.* **2018**, *8*, 1801698. [CrossRef]
24. Li, S.; Xu, Y.; Chen, Y.; Li, W.; Lin, L.; Li, M.; Deng, Y.; Wang, X.; Ge, B.; Yang, C.; et al. Tuning the selectivity of catalytic carbon dioxide hydrogenation over iridium/cerium oxide catalysts with a strong metal-support interaction. *Angew. Chem. Int. Ed.* **2017**, *56*, 10761–10765. [CrossRef]
25. Sun, H.; Ding, Z.; Sun, H.; Li, S.; Lavernia, E.J.; Liu, W. The synergistic effects of energy barriers and shear directions on twinning in face centered cubic metals. *Comput. Mater. Sci.* **2020**, *177*, 1095477. [CrossRef]
26. Guo, F.; Zou, Z.; Zhang, Z.; Zeng, T.; Tan, Y.; Chen, R.; Wu, W.; Cheng, N.; Sun, X. Confined sub-nanometer PtCo clusters as a highly efficient and robust electrocatalyst for the hydrogen evolution reaction. *J. Mater. Chem. A* **2021**, *9*, 5468–5474. [CrossRef]
27. Strickler, A.L.; Flores, R.A.; King, L.A.; Norskov, J.K.; Bajdich, M.; Jaramillo, T.F. Systematic investigation of iridium-based bimetallic thin film catalysts for the oxygen evolution reaction in acidic media. *ACS Appl. Mater. Interfaces* **2019**, *11*, 34059–34066. [CrossRef]
28. Fang, D.; Tang, X.; Yang, L.; Xu, D.; Zhang, H.; Sun, S.; Shao, Z.; Yi, B. Facile synthesis of Pt-decorated Ir black as a bifunctional oxygen catalyst for oxygen reduction and evolution reactions. *Nanoscale* **2019**, *11*, 9091–9102. [CrossRef]
29. Lim, J.; Park, D.; Jeon, S.S.; Roh, C.-W.; Choi, J.; Yoon, D.; Park, M.; Jung, H.; Lee, H. Ultrathin IrO_2 nanoneedles for electrochemical water oxidation. *Adv. Funct. Mater.* **2018**, *28*, 1704796. [CrossRef]
30. Sharma, L.; Katiyar, N.K.; Parui, A.; Das, R.; Kumar, R.; Tiwary, C.S.; Singh, A.K.; Halder, A.; Biswas, K. Low-cost high entropy alloy (HEA) for high-efficiency oxygen evolution reaction (OER). *Nano Res.* **2021**, *15*, 4799–4806. [CrossRef]
31. Zhu, K.; Wu, T.; Li, M.; Lu, R.; Zhu, X.; Yang, W. Perovskites decorated with oxygen vacancies and Fe-Ni alloy nanoparticles as high-efficiency electrocatalysts for the oxygen evolution reaction. *J. Mater. Chem. A* **2017**, *5*, 19836–19845. [CrossRef]
32. Najafi, L.; Bellani, S.; Oropesa-Nuñez, R.; Martín-García, B.; Prato, M.; Mazánek, V.; Debellis, D.; Lauciello, S.; Brescia, R.; Sofer, Z.; et al. Niobium disulphide (NbS_2)-based (heterogeneous) electrocatalysts for an efficient hydrogen evolution reaction. *J. Mater. Chem. A* **2019**, *7*, 25593–25608. [CrossRef]
33. Ahmed, J.; Alhokbany, N.; Ahamad, T.; Alshehri, S.M. Investigation of enhanced electro-catalytic HER/OER performances of copper tungsten oxide@reduced graphene oxide nanocomposites in alkaline and acidic media. *New J. Chem.* **2022**, *46*, 1267–1272. [CrossRef]
34. Ling, Y.; Kazim, F.M.D.; Zhang, Q.; Xiao, S.; Li, M.; Yang, Z. Construction of Mo_2C/W_2C heterogeneous electrocatalyst for efficient hydrogen evolution reaction. *Int. J. Hydrog. Energy* **2021**, *46*, 9699–9706. [CrossRef]
35. Jing, Y.; Liu, H.; Yan, R.; Chen, J.; Dai, H.; Liu, C.; Zhang, X.-D. Mesoporous CoP Nanowire Arrays for Hydrogen Evolution. *ACS Appl. Nano Mater.* **2019**, *2*, 5922–5930. [CrossRef]
36. Tong, J.; Li, T.; Bo, L.; Li, W.; Li, Y.; Zhang, Q. Greatly improved HER electrocatalytic activity by the composite of $CoSe_2$ and N, S-dual doped graphitic carbon. *Int. J. Hydrog. Energy* **2019**, *44*, 13424–13431. [CrossRef]